Nanoscale

PAPER

Cite this: *Nanoscale*, 2023, **15**, 10614

Single up-conversion nanocrystal as a local temperature probe of electrically heated silver nanowire†

K. Wiwatowski, [a] K. Sulowska, [a] R. Houssaini,[b] A. Pilch-Wróbel, [c] A. Bednarkiewicz, [c] A. Hartschuh, [b] S. Maćkowski [a] and D. Piątkowski *[a]

Received 29th March 2023,
Accepted 7th June 2023

DOI: 10.1039/d3nr01461d

rsc.li/nanoscale

Luminescence thermometry is a powerful technique for monitoring temperature in a sensitive, remote (through light), and minimally invasive manner. Up to now, many macroscopic and microscopic luminescence temperature probes exploiting different temperature sensing schemes have been investigated, with the majority of the studies using aggregates of nanothermometers. This work presents isolated single up-converting $NaYF_4:Er^{3+}/Yb^{3+}$ nanocrystals as functional temperature indicators operating in a standard confocal microscopy configuration. More specifically, the nanocrystals were used to monitor the temperature of a single silver nanowire, whose temperature was controlled electrically *via* the Joule process. We demonstrate that individual nanocrystals placed near the nanowire can precisely determine the temperature distribution in its surroundings. These results, which combine nanoscopic heat generation with temperature readout using isolated nanocrystals, represent an essential step for the application of isolated single nanoprobes for luminescence thermometry at the nanoscale.

Introduction

Knowledge of the temperature of physical systems has, for centuries, played a crucial role in exploring and understanding natural phenomena. In recent years, due to the rapid development of nanoscience, the challenge of temperature measurement is still relevant and often crucial for understanding physical effects, chemical reactions, or biological processes that take place at the micro- or nanoscale. Therefore, much attention has been paid to applying optical techniques for luminescence-based thermometry.[1,2] In particular, luminescence thermometry, which involves nanoscopic luminescent probes, yields precise local temperature readout based on the analysis of the spectral properties of the probe. Importantly, their small dimensions and minute heat capacity provide minimal impact on the investigated system and enable temperature mapping with high spatial resolution, limited only by the diffraction and/or the size of the probe.

Over the years, various nanoprobes, such as fluorescent dyes,[3,4] proteins,[5] semiconductor quantum dots,[6,7] mesoporous silica nanoparticles,[8] and other inorganic nanocrystals, such as nanodiamonds[9] or lanthanide-doped nanocrystals[10,11] have been synthesized and intensively studied in the context of luminescence thermometry. An exciting class of nanostructures for luminescence thermometry are rare-earths (REs) doped nanocrystals (NCs), which stand out with multiple spectrally narrow emission lines, long luminescence decay times, and remarkable optical stability.[12] They feature neither blinking nor bleaching of emission and thus are predisposed for precise, high-accuracy spectroscopic measurements. Additionally, some REs ions like Pr^{3+}, Nd^{3+}, Ho^{3+}, Er^{3+}, and Tm^{3+} can be efficiently excited by sequential absorption of infrared photons in the up-conversion processes.[13] Infrared excitation provides efficient penetration through scattering and absorbing samples (such as tissues), minimizes autofluorescence of the sample, and thus gives the advantage of excellent temperature readout capabilities. For this reason, REs-doped probes have found many technological and biomedical applications as temperature sensors.[14]

Of particular interest are Er^{3+}/Yb^{3+} co-activated nanocrystals, commonly used as luminescence temperature indicators.[15,16] For this material, optical temperature readout is typically realized by spectral analysis of the green lumine-

[a]*Institute of Physics, Faculty of Physics, Astronomy and Informatics, Nicolaus Copernicus University in Toruń, ul. Grudziądzka 5, 87-100 Toruń, Poland. E-mail: dapi@fizyka.umk.pl*
[b]*Department of Chemistry and Center for NanoScience (CeNS), LMU Munich, Butenandtstr. 5-13, 81377 Munich, Germany*
[c]*Institute of Low Temperature and Structure Research, Polish Academy of Sciences, Okólna 2, 50-422 Wroclaw, Poland*

† Electronic supplementary information (ESI) available. See DOI: https://doi.org/10.1039/d3nr01461d

scence of Er^{3+}, positioned between 520 and 560 nm.[17] This emission band consists of two close-lying lines assigned to f → f electric-dipole transitions $^2H_{11/2} \rightarrow {}^4I_{15/2}$, the H band, and $^4S_{3/2} \rightarrow {}^4I_{15/2}$, the S band (Fig. 1a). The energy gap (ΔE) between $^2H_{11/2}$ and $^4S_{3/2}$ levels is relatively small, typically around several hundred cm^{-1}.[18] In this way, both the luminescence intensity ratio (LIR) of the H and S band and the population ratio are driven by the local temperature, according to the Boltzmann equation[19]

$$\mathrm{LIR} = \frac{I_H}{I_S} \propto \frac{N(^2H_{11/2})}{N(^4S_{3/2})} \propto \exp\left(\frac{-\Delta E}{k_B T}\right) \quad (1)$$

where I_H and I_S represent the intensity of the H and the S band, respectively, N describes the population density of the particular state, and k_B is the Boltzmann constant. Thus, any temperature rise populates the high-lying $^2H_{11/2}$ state at the expense of the low-lying $^4S_{3/2}$, which changes the intensity ratio of the H and S emission bands, and modifies the emission spectrum, as schematically presented in Fig. 1b. Erbium and ytterbium co-doped nanocrystals have found numerous applications in the temperature sensing, including outstanding realizations like near-field thermal imaging[20] or intracellular temperature sensing.[21] Until today, it has not been explicitly demonstrated that single up-converting nanocrystal can be successfully used as high-sensitivity temperature probes with the same sensitivity as their ensembles.

The key prerequisite for a suitable experimental design to address this challenge concerns, in addition to measuring the optical response of a single up-converting nanocrystal, the ability to heat locally. Indeed, it is clear that in order to evaluate the robustness and reliability of temperature measurements with high spatial resolution, *i.e.*, on a single nanocrystal level, any homogenous volumetric sample heating approach would be inappropriate. Therefore, it is important to devise ways to control the temperature at a spatial scale comparable to that of the probe. Up to date, only a few sub-microscale heating techniques have been presented. Among them, relatively easily accessible are optical techniques involving interactions between light and various metallic nanoparticles.[22,23] Apart from laser heating, which produces optical noise potentially disturbing a single luminescent nanoprobe, electrically controlled metallic structures heating at the micro- and sub-microscale appear to be very interesting.[20] In recent years, many promising approaches utilizing current-induced Joule heating in silver nanowires (AgNWs) have been presented, and their heating capabilities have been studied.[24–26] For instance, a random network of silver nanowires was used for thin-film heater fabrication, featuring high-temperature stability and excellent performance.[27,28] Another time, AgNWs have been used as thermochemical nanoreactors to precisely control the growth of ZnO nanostructures.[29] In this case, nanowires showed great potential as a heat source capable of controlling chemical reactions *in situ*, literally at the nanoscale. Last but not least, electrically heated silver nanowire networks have been used for exploring the thermal properties of various up-conversion nanomaterials.[30,31]

In this work, we assemble a heat source based on a single AgNW to measure the temperature in its vicinity using a single up-conversion nanocrystal. In this experiment, the physical properties and parameters of nanowires are the key issue. Since their diameters are comparable to the size of the luminescence nanoprobes, their thermal impact is also spatially well-defined. At the same time, their lengths of tens of micrometers are highly advantageous, as the AgNWs can be easily observed or even manipulated under the optical microscope. In particular, the AgNWs can be electrically biased, and at the same time, they feature no inherent luminescence, limiting any interference with the optical response of the nanothermometer. On the contrary, under optimal circumstances, the luminescence response of a single emitter placed in the vicinity of an AgNW can be significantly enhanced due to plasmonic effects.[32]

Explicit demonstration of the sensoric properties of perfectly isolated, single up-converting nanocrystals is achieved by placing them at distances of up to a few micrometers from a

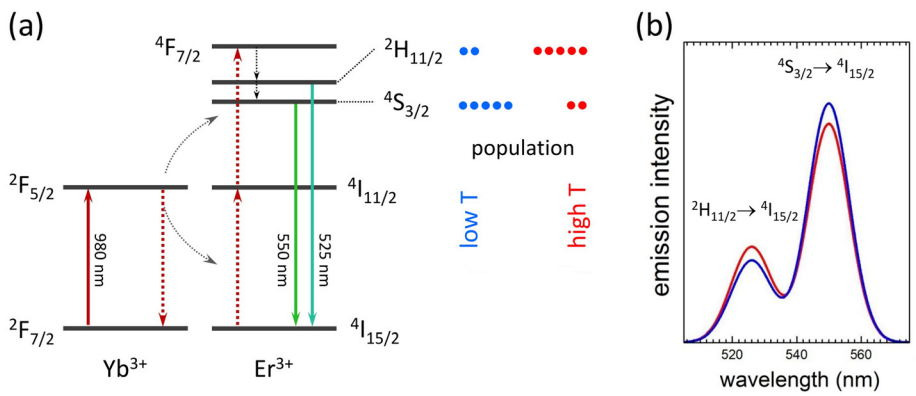

Fig. 1 (a) Illustrative energy diagram of the Er^{3+}/Yb^{3+} system together with the up-converting excitation scheme leading to the activation of the green emission of Er^{3+}. Note the thermally controlled population ratio of $^4S_{3/2}$ and $^2H_{11/2}$ levels. (b) Modeled impact of a temperature rise on the Er^{3+} green luminescence spectrum.

single AgNW, whose heating was controlled in an electrically-driven Joule process. Using conventional confocal microscopy, we have shown that individual nanocrystals can precisely measure the temperature in the vicinity of the nanowire. Indeed, upon increasing the current through the AgNW, we find a monotonic change of the up-conversion luminescence spectrum of a single nanocrystal. Experimental results confirm that we obtained high repeatability, long-term stability, and nanoscale precision of spatial positioning of the temperature readout.

Methodology

Luminescence probes

As temperature nanosensors, erbium(III) and ytterbium(III) co-doped sodium yttrium fluoride nanocrystals were used. Owing to a ladder of absorption lines,[33] visible photoluminescence (PL) of Er^{3+} can be activated both in the ultraviolet (f–d transitions) or in the visible (f–f transitions) spectral range.[12] Due to the presence of sensitizing Yb^{3+} ions, also near-infrared excitation can efficiently activate visible PL in the up-conversion process.[34] In particular, a laser operating at 980 nm excites ytterbium ions (donors), the energy is then transferred to erbium ions (acceptors) and activates the luminescence. The green emission of Er^{3+} can be excited *via* all of the above excitation channels and can be exploited for temperature readout.[2]

The nanocrystals were prepared by a wet chemistry method: in the first step, the core material was synthesized using the already described protocol.[35–37] The obtained $NaYF_4$ cores consist of 2 mol% of Er^{3+} and 20 mol% of Yb^{3+}, offering efficient up-conversion luminescence. At this stage, the cores are fully optically operative and will not be further changed. However, to prevent luminescence quenching by the solvent or other unspecific surfactants, the cores were coated with an optically passive layer of undoped $NaYF_4$ in the additional synthesis procedure.[38–40] Eventually, the obtained core@shell NCs are optically stable and not susceptible to external factors. The final product of the reaction was dispersed in chloroform.

The morphology and microstructure of the NCs were investigated with transmission electron microscopy (Philips CM20 SuperTwin). The NCs feature a quasi-spherical shape with an average diameter of about 22 nm (core) and about 9 nm (on average) thin shell (Fig. 2a and Fig. S1, ESI†). Due to the high uniformity of the host matrix, no structural transition between the core and the shell structure is noticeable. The crystalline structure of NCs was investigated by X-ray diffraction (X'Pert PRO). The measured XRD patterns were assigned using the International Centre for Diffraction Data (ICDD) database. Observed reflexes (Fig. 2b) can be identified as the pure hexagonal (β) phase of the $NaYF_4$ crystal (no. 04-011-3581).

Nanoheaters

We used single silver nanowires as well-defined microscopic heaters. They were prepared using the polyol process, a straightforward and affordable synthesis procedure.[41] The obtained nanowires have lengths from a few to several dozen micrometers and an average diameter of about 120 nm (Fig. 2c and Fig. S2, ESI†). First, the solution of AgNWs was examined optically by analyzing its extinction spectrum. Colloidal dilution of good quality nanowires in water shows an extinction spectrum with a maximum at about 400 nm.[42] Afterward, the quality of the crystalline structure of individual AgNWs was examined experimentally, analyzing the propagation length of the light-activated surface plasmon polaritons.[43] Only high-quality nanowires, free of local defects, with propagating lengths reaching dozens of micrometers, were used for further experiments, as they require high thermal and electrical conductivity.

Experimental setup

The key optical experiments were performed using a custom-built confocal luminescence microscope (Eclipse Ti-S, Nikon, Japan), optimized for detecting up-converting photoluminescence (Fig. 3). Nanocrystals were excited using a continuous-wave laser diode operating at 980 nm with light coupled to a single mode fiber. The excitation beam was colli-

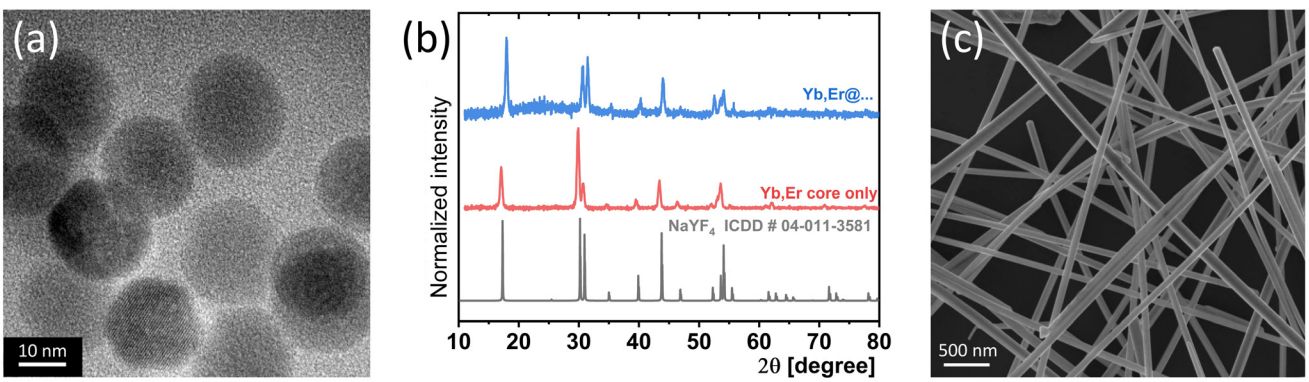

Fig. 2 (a) Transmission electron microscopy image together with (b) X-ray diffraction patterns of Er^{3+}/Yb^{3+} doped core@shell nanocrystals. (c) Scanning electron microscopy image of silver nanowires.

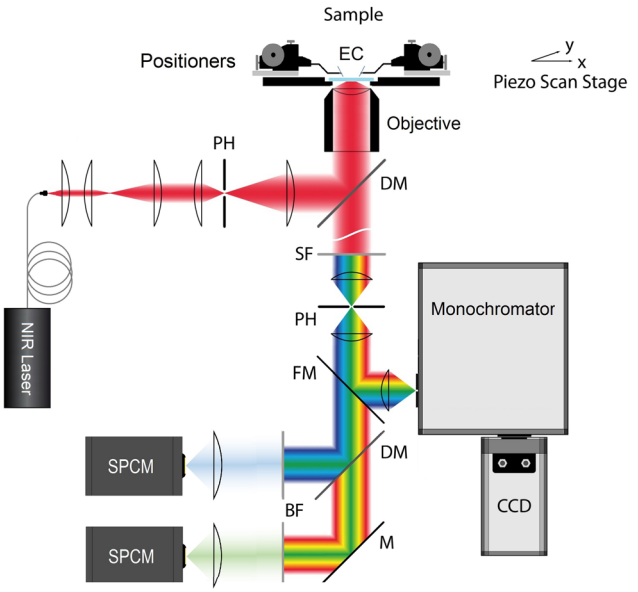

Fig. 3 Sketch of the experimental setup, where: M – mirror, PH – pinhole, EC – electrical contacts, DM – dichroic mirror, SF – short-pass filter, FM – flip mirror, BF – band-pass filter, SPCM – single photon counting module.

mated and directed to a high numerical aperture oil-immersed objective (Plan Apo 60×, NA = 1.40, Nikon, Japan) using a dichroic mirror (675dcspxr, Chroma, USA). The resulting excitation spot was about 430 nm in diameter, determining the optical resolution of the system.[44] The luminescence signal was collected by the same objective, it was first collimated and then focused onto the confocal aperture (d = 25 μm), and later directed toward the detector.

Luminescence spectra, crucial for temperature readout, were measured by a Czerny-Turner monochromator (Shamrock 500i, Andor, UK) equipped with a back-illuminated Electron Multiplying CCD camera (Newton, Andor Technology, UK) capable of single NC luminescence detection. Alternatively, the luminescence was redirected to the set of two Single Photon Counting Modules (COUNT-100, Laser Components, Germany), SPCMs, following dichroic mirror (HC BS R532, Semrock, USA). The role of the dichroic mirror was the spectral separation of the two green Er^{3+} bands used for temperature readout. Band-pass filters centered at 520 nm (Z520/20×, Chroma, USA) and 550 nm (FB550/40, Thorlabs, USA) mounted in front of SPCMs were used for final filtering. The sample holder was integrated with a piezoelectric stage (P-517, Physik Instrumente, Germany) and mounted on the top of the microscope body.

SPCMs were synchronized with the piezoelectric stage using a multifunctional I/O PC card (PCI-6236, National Instruments, USA) for photoluminescence raster scanning. PL intensity maps could be acquired in a maximal range of 100 × 100 μm^2 with a minimum step size of the piezoelectric stage much better than the optical resolution of the system.

The local temperature was controlled by a single AgNW and the Joule heating process. The heating control system consisted of two micropositioners (DPP220, Cascade Microtech, USA), each with an arm equipped with a tungsten tip approaching the sample. Positioners were firmly attached to the top plate of the microscope, giving access to the sample from above. The electric circuit was powered by a programmable power supply (DP831A, Rigol, China), operating in the range of single milliampere. The process of approaching the selected silver nanowire with the probe tips was monitored in real-time utilizing a wide-field white light transmission mode and a CCD camera (1501C, Thorlabs, USA).

The sample was prepared as follows. First, a small fraction of synthesized NWs colloid was diluted in deionized water to lower their density. Afterward, about 40 μl of concentration-optimized colloid was spin-coated at 5000 rpm for 45 seconds on a glass coverslip. The achieved surface density of the AgNWs was about 2–3 nanowires per 250 μm^2. Next, 20 μl of diluted colloid of NCs in chloroform was spin-coated for 5 s at 2500 rpm on the same sample. The colloid concentration was lowered to achieve the surface density of the NCs about 10–20 particles per 250 μm^2. Such a procedure resulted in well-separated silver nanowires and single nanocrystals distributed over the whole coverslip area, with some fraction of isolated NCs, deposited in the close vicinity of the nanowires.

Results and discussion

First, the luminescence response of nanocrystals exposed to well-known temperatures was calibrated. For this purpose, a transparent heating glass plate (ThermoPlate, Tokai Hit, Japan) placed less than 1 mm over the sample (nanocrystals) was used. The temperature of the thermoplate was stabilized automatically with an accuracy of 0.3 °C and monitored by a built-in sensor. Since the oil-immersion objective was very sensitive to macroscopic temperature fluctuations induced by the thermoplate, for calibrations we used an air objective (S Plan Fluor, 60×, NA = 0.70, Nikon, Japan), in order to minimize heat conductivity between the sample and the objective. Because the low aperture objective reduces the sensitivity of the optical detection, the calibration procedure was performed using small agglomerates of NCs giving about 10 times higher PL signal-to-noise ratio. Such an approach is justified since in core–shell nanocrystals the optically active core is effectively isolated even from the surfactants.[45] Therefore, any interaction between nearby NCs is impossible and their spectral response does not depend on their local concentration.

It has been demonstrated that under 980 nm laser illumination Er^{3+}/Yb^{3+} activated nanocrystals can also warm up.[46] As any laser-stimulated temperature rise is strongly unwanted in the temperature sensing experiment, we placed great care on careful optimization of the excitation laser power density. Detailed analysis of single NCs emission spectrum shows no thermal modification of the S and H band relative intensities for the laser powers up to 500 μW (ρ = 3.5 mW μm^{-2}) measured before the objective. At the same time, such an excitation power ensures reasonable spectra acquisition time (5 s)

and a signal-to-noise ratio (SNR) of about 15, providing good-quality emission spectra of single nanocrystals.

The calibration luminescence spectra were acquired in a precisely controlled temperature range, from 25 °C to 50 °C with a step of 5 °C. We assumed no significant heat losses on a millimeter distance between the macroscopic thermoplate and the sample surface. For each step, the natural logarithm of the LIR has been plotted *versus* the reciprocal of the temperature (Arrhenius plot) and presented in Fig. 4a. The experimental points were fitted by a linear function

$$\ln(\mathrm{LIR}) = -\frac{\Delta E}{k_B T} + C \quad (2)$$

where the slope $\Delta E/k_B$ = 950 ± 15 K and C = 1.56 ± 0.05. The estimated energy gap ΔE is about 665 ± 15 cm^{-1} which agrees with previous spectroscopic observations in the same material.[47] The uncertainties of the fitted parameters were calculated based on the SNR of the acquired spectra using the uncertainty propagation theorem.[48] The LIR and relative sensitivity S_r = 100% × $\Delta E k_B^{-1} T^{-2}$ calculated for a temperature range from 250 to 400 K are presented in Fig. 4b. Note that the 1–1.5% K^{-1} relative sensitivity is achieved in the temperature range interesting for biological applications.

The nanowire, serving as a microscopic heat source, was coupled with an external current source in a multistep procedure. First, the tip probes were positioned close to the ends of a chosen nanowire. Next, they were slowly lowered toward the surface, where the contact moment between the nanowire ends and tip probes were continuously monitored under the microscope. When the circuit was closed, a clear current signal was observed. For typical heating operations, the current values reached up to 10–15 mA, depending on nanowire quality and length. Exceeding this range usually results in destroying the nanowire. An exemplary single silver nanowire observed before and after the connection with the electrical circuit is presented in Fig. 5.

The sample containing both up-converting nanocrystals and silver nanowires was assembled in a random way, as shown in Fig. 6. Few randomly oriented single nanowires can be seen, including a well-isolated, about 60 μm long nanowire placed in the middle of Fig. 6a. The positions of the nanowires were determined by mapping the spatial distribution of the backscattered (BS) laser light recorded in the confocal configuration. The same area observed in the PL imaging mode (λ_{det} = 550/40 nm) shows several well-separated single NCs, visible as bright spots in Fig. 6b. Their luminescence intensity

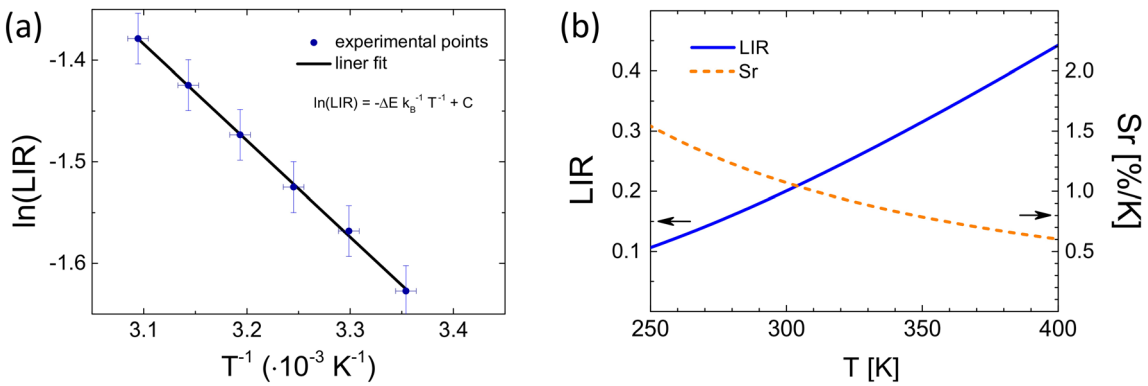

Fig. 4 (a) Natural logarithm of the luminescence intensity ratio (LIR) plotted *versus* the reciprocal of temperature used for the calibration procedure. (b) Calculated LIR and relative sensitivity (Sr) plotted *versus* temperature in the temperature range from 250 to 400 K.

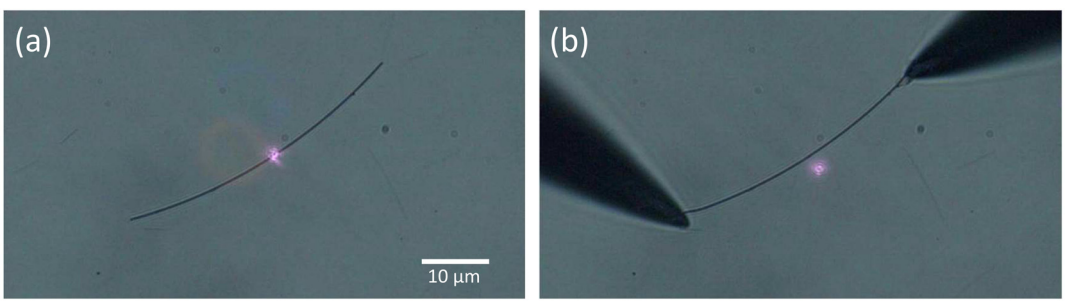

Fig. 5 (a) Single silver nanowire deposited on a glass coverslip, observed under the optical microscope in a white light transmission mode. (b) The same nanowire is connected to the current source *via* tungsten tip probes attached to the NW ends. The laser spot (pink) indicates the position of the sample over the objective. The sample holder could be freely moved in the range of about 100 μm, both for *X* and *Y* directions, with about 5 nm precision.

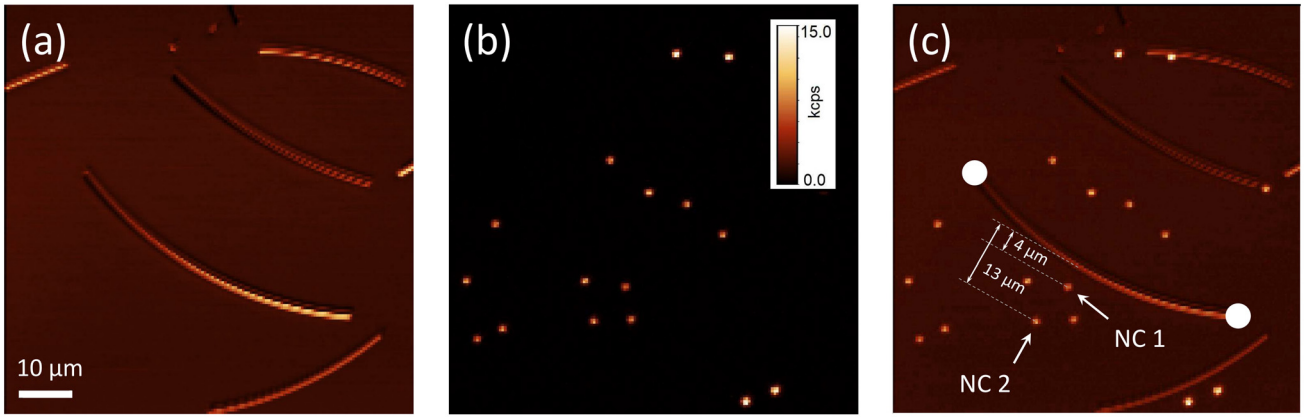

Fig. 6 (a) Single silver nanowires distributed over the sample, observed in the backscattered laser light (λ_{exc} = 980 nm) mode, (b) PL up-conversion intensity map (λ_{exc} = 980 nm, λ_{det} = 550/40 nm) of the single nanocrystals spin-coated on the sample, (c) superposition of the image (a) and (b) illustrating the geometry of the sample. The NC1 and NC2 are localized 4 μm and 13 μm away from the nanowire, respectively. White spots indicate the positions of the electrical tip probes.

reaches about 10 kcps, sufficient for carrying out single nanocrystal spectroscopic temperature measurements.

As nanoscopic temperature indicators, single NCs deployed around a single silver nanowire were used. The mutual spatial orientation between NWs and NCs is seen in Fig. 6c, which combines BS and PL maps. We correlated the nanocrystals and single nanowire positions and chose nanocrystals that were sufficiently close to the electrically connected nanowire – the heat source. In the following, we focus on the nanocrystals labeled NC1 and NC2, positioned collinearly in the middle of the nanowire at distances of 4 μm and 13 μm, respectively, and exposed to the local temperature gradient.

The luminescence spectra of NC1 and NC2 exposed to the maximal available temperature (I = 10 mA) together with the reference spectrum (room temperature) are presented in Fig. 7a. Measured spectra consist of two well-defined H and S bands, centered at 525 and 550 nm, respectively, which relative intensity can be controlled by the local temperature. Each band, however, shows narrow peaks attributed to the levels split by the crystal field of the host matrix.[49] Additionally, the temperature was monitored in real-time by comparing the relative intensities of H and S bands by two SPCMs.

The key observation reported here is that the intensity of the H band apparently increases with a simultaneous decrease of the S band intensity as a function of the current driven through the silver nanowire. As driving the current results in nanowire heating, we attribute this spectral behavior as resulting from the temperature changes in the vicinity of the nanowire. Such behavior follows the model presented

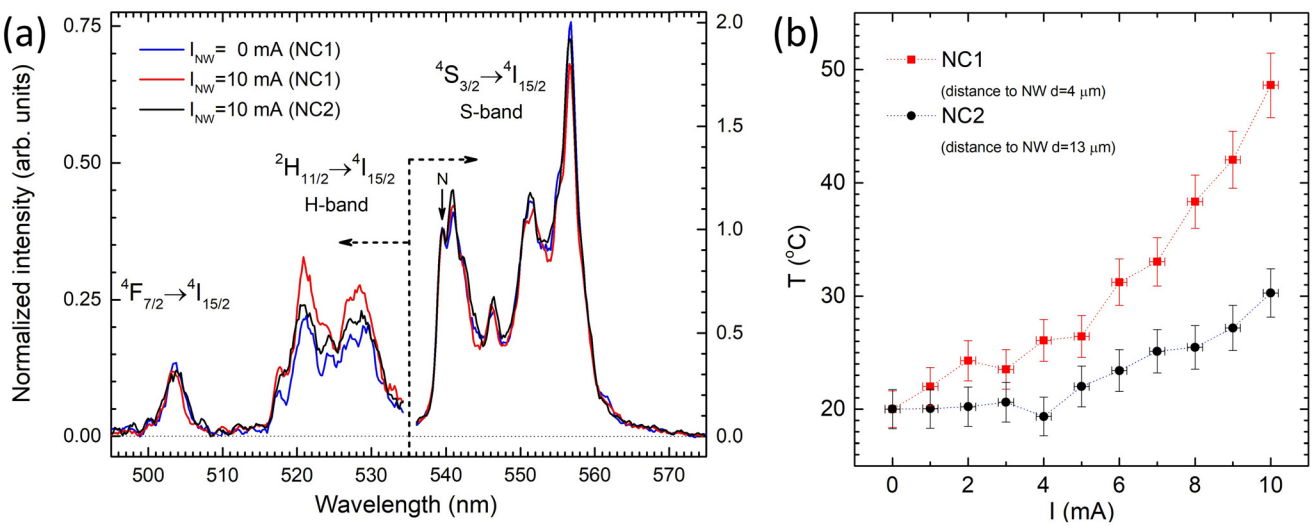

Fig. 7 (a) Normalized luminescence spectra of single NCs (NC1 and NC2) exposed to a single nanowire Joule heating. The spectral intensities are normalized at λ_N = 540 nm. (b) The temperature readout of NC1 and NC2 made for several temperatures of the nanowire plotted *versus* the applied current.

in Fig. 2. The most temperature-sensitive transition within the S band is the long-wavelength one at 557 nm, attributed to the emission from the lowest crystal level of the $^4S_{3/2}$ multiplet. On the other hand, a worth noticing weak line centered at 504 nm and attributed to the $^4F_{7/2} \rightarrow {}^4I_{15/2}$ transitions exhibit essentially no change as a function of the electric current in the nanowire. This insensitivity is expected as the $^4F_{7/2}$ level cannot be populated thermally in this experiment. Importantly, it demonstrates the stability and repeatability of the measurement.

The emission spectra of NC1 and NC2 were measured systematically for several current values with 1 mA step, up to 10 mA. Higher currents were not applied to avoid any damage to the nanowire. The H and S band intensities were integrated for each value of the current, and the temperature was calculated according to eqn (2) using determined calibration parameters. Temperature readouts are plotted in Fig. 7b for both selected nanocrystals as a function of the applied current. Notice the monotonic temperature rise observed for both nanocrystals. Starting from room temperature (20 °C), NC1 placed 4 μm from the NWs achieves about 50 °C for 10 mA, whereas NC2, distant by 13 μm heats up to about 30 °C. The 20 °C temperature gradient can be attributed to the different distances from the nanowire and, thus, different heat conductivity and dissipation. The core–shell architecture of the nanocrystals ensured a high signal-to-noise ratio of the temperature readout, despite relatively small NCs being used. Indeed, small nanocrystals, due to the large surface-to-volume ratio, may frequently suffer from quenching of the luminescence by nearby surfactants.[36] In this work, similar parasitic effects have not been observed due to effective shell protection.

Conclusions

In this work, we demonstrated a functional technique for monitoring temperature at the nanoscale. The temperature readout was realized by spectroscopic analysis of individual *ca.* 20 nm (core) large erbium and ytterbium ions co-doped nanocrystals. Individual thermometer nanocrystals were dispersed around a single silver nanowire that served as a microscopic heat source. The nanowire was connected to an external milliampere range power supply, warming up in the Joule process, and controlling the temperature of the nanowire and its vicinity. Careful analysis of nanocrystal emission spectra showed several dozen Celsius degrees of the temperature gradient around the nanowire. A high signal-to-noise ratio and high sensitivity were achieved primarily due to the efficient anti-Stokes excitation mechanism of the nanocrystals operating in the up-conversion mode as well as the high thermal stability of the single silver nanowire.

Conflicts of interest

There are no conflicts to declare.

Acknowledgements

This research was financed from Project No. 2018/31/G/ST3/03596 (SM, DP, KW) founded by the National Science Centre (NCN), Poland, and HA4405/10-1 (AH, RH) founded by the German Research Foundation (DFG). KS was supported by NCN Project No. 2021/41/N/ST7/03528. The AB and APW work was financially supported with the statutory funds of the Institute of Low Temperature and Structure Research, Polish Academy of Sciences, Wrocław, Poland.

References

1 M. Dramicanin, *Luminescence Thermometry: Methods, Materials, and Applications*, Woodhead Publishing, 2018.
2 D. Jaque and F. Vetrone, Luminescence Nanothermometry, *Nanoscale*, 2012, **4**(15), 4301–4326, DOI: **10.1039/C2NR30764B**.
3 J. J. Shah, M. Gaitan and J. Geist, Generalized Temperature Measurement Equations for Rhodamine B Dye Solution and Its Application to Microfluidics, *Anal. Chem.*, 2009, **81**(19), 8260–8263, DOI: **10.1021/ac901644w**.
4 C. E. Estrada-Pérez, Y. A. Hassan and S. Tan, Experimental Characterization of Temperature Sensitive Dyes for Laser Induced Fluorescence Thermometry, *Rev. Sci. Instrum.*, 2011, **82**(7), 074901, DOI: **10.1063/1.3590929**.
5 J. S. Donner, S. A. Thompson, M. P. Kreuzer, G. Baffou and R. Quidant, Mapping Intracellular Temperature Using Green Fluorescent Protein, *Nano Lett.*, 2012, **12**(4), 2107–2111, DOI: **10.1021/nl300389y**.
6 P. Haro-Gonzalez, W. T. Ramsay, L. Martinez Maestro, B. del Rosal, K. Santacruz-Gomez, M. C. Iglesias-de la Cruz, F. Sanz-Rodriguez, J. Y. Chooi, P. Rodriguez-Sevilla, M. Bettinelli, D. Choudhury, A. K. Kar, J. Garcia Sole, D. Jaque and L. Paterson, Quantum Dot Based Thermal Spectroscopy and Imaging of Optically Trapped Micro-Spheres and Single Cells, *Small*, 2013, **9**(12), 2162–2170, DOI: **10.1002/smll.201201740**.
7 G. W. Walker, V. C. Sundar, C. M. Rudzinski, A. W. Wun, M. G. Bawendi and D. G. Nocera, Quantum-Dot Optical Temperature Probes, *Appl. Phys. Lett.*, 2003, **83**(17), 3555–3557, DOI: **10.1063/1.1620686**.
8 A. M. Kaczmarek, M. Suta, H. Rijckaert, A. Abalymov, I. Van Driessche, A. G. Skirtach, A. Meijerink and P. Van Der Voort, Visible and NIR Upconverting Er3+–Yb3+ Luminescent Nanorattles and Other Hybrid PMO-Inorganic Structures for In Vivo Nanothermometry, *Adv. Funct. Mater.*, 2020, **30**(32), 2003101, DOI: **10.1002/adfm.202003101**.
9 E. Glushkov, V. Navikas and A. Radenovic, Fluorescent Nanodiamonds as Versatile Intracellular Temperature Sensors, *Chimia*, 2019, **73**(1–2), 73–73, DOI: **10.2533/chimia.2019.73**.
10 A. Bednarkiewicz, L. Marciniak, L. D. Carlos and D. Jaque, Standardizing Luminescence Nanothermometry for

Biomedical Applications, *Nanoscale*, 2020, **12**(27), 14405–14421, DOI: 10.1039/D0NR03568H.

11 P. S. Solanki, S. Balabhadra, M. F. Reid, V. B. Golovko and J.-P. R. Wells, Upconversion Thermometry Using Yb3+/Er3+ Co-Doped KY3F10 Nanoparticles, *ACS Appl. Nano Mater.*, 2021, **4**(6), 5696–5706, DOI: 10.1021/acsanm.1c00353.

12 G. Blasse and B. C. Grabmaier, *Luminescent Materials*, Springer-Verlag, 1994.

13 F. Auzel, Upconversion and Anti-Stokes Processes with f and d Ions in Solids, *Chem. Rev.*, 2004, **104**(1), 139–174, DOI: 10.1021/cr020357g.

14 A. Bednarkiewicz, J. Drabik, K. Trejgis, D. Jaque, E. Ximendes and L. Marciniak, Luminescence Based Temperature Bio-Imaging: Status, Challenges, and Perspectives, *Appl. Phys. Rev.*, 2021, **8**(1), 011317, DOI: 10.1063/5.0030295.

15 L. T. K. Giang, K. Trejgis, L. Marciniak, N. Vu and L. Q. Minh, Fabrication and Characterization of Up-Converting β-NaYF4:Er3+,Yb3+@NaYF4 Core–Shell Nanoparticles for Temperature Sensing Applications, *Sci. Rep.*, 2020, **10**(1), 14672, DOI: 10.1038/s41598-020-71606-6.

16 A. M. Kaczmarek, M. Suta, H. Rijckaert, T. P. van Swieten, I. V. Driessche, M. K. Kaczmarek and A. Meijerink, High Temperature (Nano)Thermometers Based on LiLuF4:Er3+, Yb3+ Nano- and Microcrystals. Confounded Results for Core–Shell Nanocrystals, *J. Mater. Chem. C*, 2021, **9**(10), 3589–3600, DOI: 10.1039/D0TC05865C.

17 M. A. Antoniak, S. J. Zelewski, R. Oliva, A. Żak, R. Kudrawiec and M. Nyk, Combined Temperature and Pressure Sensing Using Luminescent $NaBiF_4$:Yb,Er Nanoparticles, *ACS Appl. Nano Mater.*, 2020, **3**(5), 4209–4217, DOI: 10.1021/acsanm.0c00403.

18 W. T. Carnall, P. R. Fields and B. G. Wybourne, Spectral Intensities of the Trivalent Lanthanides and Actinides in Solution. I. Pr3+, Nd3+, Er3+, Tm3+, and Yb3+, *J. Chem. Phys.*, 1965, **42**(11), 3797–3806, DOI: 10.1063/1.1695840.

19 S. Drobczyński, K. Prorok, K. Tamarov, K. Duś-Szachniewicz, V.-P. Lehto and A. Bednarkiewicz, Toward Controlled Photothermal Treatment of Single Cell: Optically Induced Heating and Remote Temperature Monitoring In Vitro through Double Wavelength Optical Tweezers, *ACS Photonics*, 2017, **4**(8), 1993–2002, DOI: 10.1021/acsphotonics.7b00375.

20 L. Aigouy, G. Tessier, M. Mortier and B. Charlot, Scanning Thermal Imaging of Microelectronic Circuits with a Fluorescent Nanoprobe, *Appl. Phys. Lett.*, 2005, **87**(18), 184105, DOI: 10.1063/1.2123384.

21 X. Di, D. Wang, J. Zhou, L. Zhang, M. H. Stenzel, Q. P. Su and D. Jin, Quantitatively Monitoring In Situ Mitochondrial Thermal Dynamics by Upconversion Nanoparticles, *Nano Lett.*, 2021, **21**(4), 1651–1658, DOI: 10.1021/acs.nanolett.0c04281.

22 A. O. Govorov and H. H. Richardson, Generating Heat with Metal Nanoparticles, *Nano Today*, 2007, **2**(1), 30–38, DOI: 10.1016/S1748-0132(07)70017-8.

23 G. Baffou, *Thermoplasmonics: Heating Metal Nanoparticles Using Light*, Cambridge University Press, Cambridge, United Kingdom; New York, NY, 2017.

24 Y. Huang, Y. Tian, C. Hang, Y. Liu, S. Wang, M. Qi, H. Zhang and J. Zhao, Self-Limited Nanosoldering of Silver Nanowires for High-Performance Flexible Transparent Heaters, *ACS Appl. Mater. Interfaces*, 2019, **11**(24), 21850–21858, DOI: 10.1021/acsami.9b06029.

25 H. H. Khaligh, L. Xu, A. Khosropour, A. Madeira, M. Romano, C. Pradére, M. Tréguer-Delapierre, L. Servant, M. A. Pope and I. A. Goldthorpe, The Joule Heating Problem in Silver Nanowire Transparent Electrodes, *Nanotechnology*, 2017, **28**(42), 425703, DOI: 10.1088/1361-6528/aa7f34.

26 C.-L. Kim, J.-Y. Lee, D.-G. Shin, J.-S. Yeo and D.-E. Kim, Mechanism of Heat-Induced Fusion of Silver Nanowires, *Sci. Rep.*, 2020, **10**(1), 9271, DOI: 10.1038/s41598-020-66304-2.

27 J. C. Lee, J. Min, P. J. Jesuraj, H. Hafeez, D. H. Kim, W. H. Lee, D. K. Choi, J. H. Cha, C. M. Lee, M. Song, C. S. Kim and S. Y. Ryu, Improved Stability of Silver Nanowire (AgNW) Electrode for High Temperature Applications Using Selective Photoresist Passivation, *Microelectron. Eng.*, 2019, **206**, 6–11, DOI: 10.1016/j.mee.2018.12.001.

28 T. Kim, Y. W. Kim, H. S. Lee, H. Kim, W. S. Yang and K. S. Suh, Uniformly Interconnected Silver-Nanowire Networks for Transparent Film Heaters, *Adv. Funct. Mater.*, 2013, **23**(10), 1250–1255, DOI: 10.1002/adfm.201202013.

29 J. Yeo, G. Kim, S. Hong, J. Lee, J. Kwon, H. Lee, H. Park, W. Manoroktul, M.-T. Lee, B. J. Lee, C. P. Grigoropoulos and S. H. Ko, Single Nanowire Resistive Nano-Heater for Highly Localized Thermo-Chemical Reactions: Localized Hierarchical Heterojunction Nanowire Growth, *Small*, 2014, **10**(24), 5015–5022, DOI: 10.1002/smll.201401427.

30 E. D. Martínez, C. D. S. Brites, L. D. Carlos, A. F. García-Flores, R. R. Urbano and C. Rettori, Electrochromic Switch Devices Mixing Small- and Large-Sized Upconverting Nanocrystals, *Adv. Funct. Mater.*, 2019, **29**(8), 1807758, DOI: 10.1002/adfm.201807758.

31 E. D. Martínez, C. D. S. Brites, L. D. Carlos, R. R. Urbano and C. Rettori, Upconversion Nanocomposite Materials With Designed Thermal Response for Optoelectronic Devices, *Front. Chem.*, 2019, **7**, 83, DOI: 10.3389/fchem.2019.00083.

32 D. Piatkowski, N. Hartmann, T. Macabelli, M. Nyk, S. Mackowski and A. Hartschuh, Silver Nanowires as Receiving-Radiating Nanoantennas in Plasmon-Enhanced up-Conversion Processes, *Nanoscale*, 2015, **7**(4), 1479–1484, DOI: 10.1039/C4NR05209A.

33 G. H. Dieke and H. M. Crosswhite, The Spectra of the Doubly and Triply Ionized Rare Earths, *Appl. Opt.*, 1963, **2**(7), 675–686, DOI: 10.1364/AO.2.000675.

34 F. Auzel, Compteur Quantique Par Transfert d'energie Entre Deux Ions de Terres Rares Dans Un Tungstate Mixte et Dans Un Verre, *C. R. Acad. Sci. Paris*, 1966, **262**, 1016.

35 A. Pilch-Wróbel, J. Zasada and A. Bednarkiewicz, The Influence of Ce3+ Codoping and Excitation Scheme on Spectroscopic Properties of NaYF4:Yb3+,Ho3+, *J. Lumin.*, 2020, **226**, 117494, DOI: **10.1016/j.jlumin.2020.117494**.

36 J. Zhao, Z. Lu, Y. Yin, C. McRae, J. A. Piper, J. M. Dawes, D. Jin and E. M. Goldys, Upconversion Luminescence with Tunable Lifetime in NaYF4:Yb,Er Nanocrystals: Role of Nanocrystal Size, *Nanoscale*, 2013, **5**(3), 944–952, DOI: **10.1039/c2nr32482b**.

37 A. Pilch, D. Wawrzyńczyk, M. Kurnatowska, B. Czaban, M. Samoć, W. Strek and A. Bednarkiewicz, The Concentration Dependent Up-Conversion Luminescence of Ho3+ and Yb3+ Co-Doped β-NaYF4, *J. Lumin.*, 2017, **182**, 114–122, DOI: **10.1016/j.jlumin.2016.10.016**.

38 A. Pilch-Wrobel, A. M. Kotulska, S. Lahtinen, T. Soukka and A. Bednarkiewicz, Engineering the Compositional Architecture of Core-Shell Upconverting Lanthanide-Doped Nanoparticles for Optimal Luminescent Donor in Resonance Energy Transfer: The Effects of Energy Migration and Storage, *Small*, 2022, **18**(18), 2200464, DOI: **10.1002/smll.202200464**.

39 A. M. Kotulska, A. Pilch-Wróbel, S. Lahtinen, T. Soukka and A. Bednarkiewicz, Upconversion FRET Quantitation: The Role of Donor Photoexcitation Mode and Compositional Architecture on the Decay and Intensity Based Responses, *Light: Sci. Appl.*, 2022, **11**, 256, DOI: **10.1038/s41377-022-00946-x**.

40 A. Pilch, C. Würth, M. Kaiser, D. Wawrzyńczyk, M. Kurnatowska, S. Arabasz, K. Prorok, M. Samoć, W. Strek, U. Resch-Genger and A. Bednarkiewicz, Shaping Luminescent Properties of Yb3+ and Ho3+ Co-Doped Upconverting Core–Shell β-NaYF4 Nanoparticles by Dopant Distribution and Spacing, *Small*, 2017, **13**(47), 1701635, DOI: **10.1002/smll.201701635**.

41 M. Olejnik, M. Twardowska, W. Zaleszczyk and S. Mackowski, Bioconjugation of Silver Nanowires with Photosynthetic Light-Harvesting Complexes, *Acta Phys. Pol., A*, 2012, **122**(2), 357–364.

42 M. Olejnik, B. Krajnik, D. Kowalska, M. Twardowska, N. Czechowski, E. Hofmann and S. Mackowski, Imaging of Fluorescence Enhancement in Photosynthetic Complexes Coupled to Silver Nanowires, *Appl. Phys. Lett.*, 2013, **102**(8), 083703, DOI: **10.1063/1.4794171**.

43 M. Ćwierzona, K. Sulowska, M. A. Antoniak, M. Żebrowski, M. Nyk, S. Maćkowski and D. Piątkowski, Precise Laser-Cutting of Single Silver Nanowires for Direct Measurement of SPPs Propagation Losses, *Appl. Phys. Lett.*, 2022, **120**(26), 261108, DOI: **10.1063/5.0095100**.

44 L. Novotny and B. Hecht, *Principles of Nano-Optics*, Cambridge University Press, 2006.

45 F. Wang, J. Wang and X. Liu, Direct Evidence of a Surface Quenching Effect on Size-Dependent Luminescence of Upconversion Nanoparticles, *Angew. Chem., Int. Ed.*, 2010, **49**(41), 7456–7460, DOI: **10.1002/anie.201003959**.

46 A. H. Li, Z. J. Sun and Q. Lü, Laser Heating Effect on the Power Dependence of Upconversion Luminescence in Er3+ -Doped Nanopowders, *J. Nanopart. Res.*, 2012, **15**(1), 1377, DOI: **10.1007/s11051-012-1377-4**.

47 C. D. S. Brites, X. Xie, M. L. Debasu, X. Qin, R. Chen, W. Huang, J. Rocha, X. Liu and L. D. Carlos, Instantaneous Ballistic Velocity of Suspended Brownian Nanocrystals Measured by Upconversion Nanothermometry, *Nat. Nanotechnol.*, 2016, **11**(10), 851–856, DOI: **10.1038/nnano.2016.111**.

48 P. Bevington and D. K. Robinson, *Data Reduction and Error Analysis for the Physical Sciences*, McGraw-Hill Education, Boston, 3rd edn, 2002.

49 M. F. Reid, Theory of Rare-Earth Electronic Structure and Spectroscopy, in *Handbook on the Physics and Chemistry of Rare Earths*, ed. J.-C. G. Bünzli and V. K. Pecharsky, Elsevier, 2016, vol. 50, pp. 47–64, DOI: **10.1016/bs.hpcre.2016.09.001**.

